Cardiovascular Engineering and Technology, Vol. 10, No. 4, December 2019 *(© 2019)* pp. 604–617
https://doi.org/10.1007/s13239-019-00434-1

Original Article

Three-Dimensional Contractile Mechanics of Artery Accounting for Curl of Axial Strip Sectioned from Vessel Wall

KEIICHI TAKAMIZAWA

Tokyo, Japan

(Received 13 November 2018; accepted 5 October 2019; published online 17 October 2019)

Associate Editor Hwa Liang Leo oversaw the review of this article.

Abstract
Purpose—It is well known that a sliced ring of arterial wall opens by a radial cut. An axial strip sectioned from arterial wall also curls into an arc. These phenomena imply that there exist residual strains in the circumferential and axial directions. How much do the axial residual strains affect the stress distributions of arterial wall? The aim of the present study is to know stress distributions of arterial wall with the residual strains under the passive and constricted conditions.
Methods—We analyzed the stress distributions under passive and constricted conditions with considering a Riemannian stress-free configuration. In the analysis, we used strain energy functions to describe the passive and active mechanical properties of artery.
Results—The present study provided distributions of stretch ratio with reference to the stress-free state (Riemannian stress-free configuration) and stress with and without the curl of axial strip of a homogenous cylindrical arterial model under the passive and constricted smooth muscle conditions. The circumferential and axial stresses with activated smooth muscle (noradrenaline 10^{-5} M) at the intraluminal pressure 16 kPa and the axial stretch ratio 1.5 with reference to the unloaded vessel decreased by 3.5 and 13.8% at the inner surface with considering the axial residual strain, respectively.
Conclusions—We have shown that the Riemannian stress-free configuration is appropriate tool to analyze stress distributions of arterial wall under passive and activated conditions with the residual stresses.

Keywords—Arteries, Residual strains, Stress distributions, Smooth muscle constriction.

INTRODUCTION

Residual stress in arterial wall has been well known.[3,8,9,23,25,26,31,32] In the earlier studies, the residual stress relieved by a radial cut from the sliced ring of the arterial wall was noted. There is an important application of the residual stress to a lumen collapse of artery[7] depending on the axial stretch. On the other hand, the residual strain relieved by curl of axial strip has been also found.[10,13,34] In the stress analysis for arterial wall, we must consider both the residual deformations to know the precise stress distributions even under physiological conditions[34] and the residual stresses might have effect on the instability of shape of artery (collapse and buckling).

Mechanical properties of arteries with constricted smooth muscles have been also well studied for a long time,[4–6,20,29] although anisotropic constitutive laws have been recently proposed as phenomenological or chemomechanical model.[1,14,18,22,24,33] Earlier studies have often used strip specimen of arteries but the recent studies have performed experiments on intact arterial segments because these are more natural mechanical loading. And more precise experiments have performed on the separated two layers (adventitia and media) because the smooth muscle cells mainly exist in the media. However, the difficulty of experiments is significantly increased and there are only a limited kind of arterial specimens for experimentation. As far as the author knows, only the human arteries under passive condition[10,12,13] and porcine coronary arteries[16,17] have been tested in the multilayer models.

The objective of the present study is to clear the effect of the axial residual strain on the distributions of stretch ratios and stresses through the wall thickness of the arterial wall under the passive and constricted

Address correspondence to Keiichi Takamizawa, Tokyo, Japan. Electronic mail: keiichi.takamizawa@gmail.com

smooth muscle conditions. In the stress analysis with smooth muscle constriction induced by agonist, we need the constitutive laws of the passive and activated conditions. In the present study, a strain energy density function for the active stresses was proposed. This is a phenomenological function for which the material parameters were determined by the biaxial pressure loading experiments considering the stretch ratio and stress distributions. This function is described in a sense of general tensor analysis, i.e., it is applicable to the case of including shear strains. An experimental result of the relaxation of axial strip with the vaso-constrictor in canine artery[20] will be qualitatively explained using the present strain energy functions for the rabbit artery.

METHODS

Experiments

Data of ten common carotid arteries of five rabbits in a previous paper[24] were used for analyses. In the present article, a typical specimen will be analyzed on the distributions of stretch ratios and stresses in the vessel wall in details. The mechanical properties under passive and constricted with noradrenaline (NA) conditions were measured.

First an arterial specimen was set in Krebs solution at 37 °C aerated with a mixture gas of 5% CO_2 and 95% O_2. It was maintained at the axial stretch ratio 1.5 and intraluminal pressure 100 mmHg for 30 min and then the pressure decreased and increased several times between + 0 and 200 mmHg to obtain the stable pressure-diameter and pressure-axial force loops. The last loops were adopted as the passive mechanical data. Second the intraluminal pressure was maintained at 100 mmHg for about 10 min and then NA was injected by one shot into the organ bath up to NA concentration of 10^{-5} M. When the diameter decrement was saturated, the pressure was decreased + 0 mmHg and then increased 200 mmHg. The data of intraluminal pressure, external diameter, and axial force were stored on PC *via* A/D convertor. The maximal constriction of smooth muscle cells of arteries is obtained with Krebs solution at NA concentration 10^{-5} M and saturated above this concentration. The mean of experimental data from ten specimens was shown in the paper.[24]

In the present study, the opening angles of ring specimen due to a radial cut and curl of axial strip from the study[34] on a porcine common carotid artery had to be used because in the experiments of the rabbit arteries residual deformations were not measured. Radii of the ring specimen opened and axial arc were estimated from results of the present study accounting for the inner and outer diameters of the rabbit under the unloaded condition. The rabbit common carotid arteries could not be separated into adventitia and media. We performed the experiments and analyses assuming the one-layer homogeneous model.

Riemannian Stress-Free Configuration

Let B denote a set of material points considered and E^3 the three-dimensional Euclidean space. We shall call a map χ from B into E^3 a configuration.[30] A current configuration is defined as a map χ_t at a current time t. We introduce a curvilinear coordinate system $\langle x^i; g_{ij}\rangle$ where i, j are integers 1, 2, or 3, x^i denote coordinates and g_{ij} components of a metric tensor. For a material point $p \in B$, χ_t is defined as a map $(p,\ t)\mapsto x$ where $x = (x^1, x^2, x^3)$. This is represented as $x = \chi_t(p)$. In the following we shall omit t because we treat only an equilibrium problem. A configuration for the unloaded state is denoted by κ. For the unloaded state we introduce a curvilinear coordinate system $\langle \xi^\alpha; \gamma_{\alpha\beta}\rangle$. The material point $p \in B$ is mapped as $\xi = (\xi^1,\ \xi^2,\ \xi^3) = \kappa(p)$. In general, the unloaded material body κB with a metric tensor $\gamma_{\alpha\beta}$ has residual stress. However, a metric tensor with components $\eta_{\alpha\beta}$ may be defined over κB to obtain the stress-free state. In this case the infinitesimally small distance ds between two points in the stress-free configuration can be determined with $ds^2 = \eta_{\alpha\beta} d\xi^\alpha d\xi^\beta$. We shall call the body $\kappa(B)$ with a metric tensor $\eta_{\alpha\beta}$ a Riemannian stress-free configuration. The Riemannian stress-free configuration may not be generally Euclidean[27,28,36] because the Riemann-Christoffel tensor may not vanish over the body $\kappa(B)$ as shown in Appendix.

Because we treated a thick-walled cylindrical vessel, a cylindrical coordinate system $x^1 = \theta$, $x^2 = z$, and $x^3 = r$ with components of a metric tensor $g_{11} = g_{\theta\theta} = r^2$, $g_{22} = g_{zz} = 1$, $g_{33} = g_{rr} = 1$, and $g_{ij} = 0$ $(i \neq j)$ was adopted. For the unloaded configuration κ, a cylindrical coordinate system $\xi^1 = \vartheta$, $\xi^2 = \zeta$, and $\xi^3 = \rho$ with $\gamma_{11} = \gamma_{\vartheta\vartheta} = \rho^2$, $\gamma_{22} = \gamma_{\zeta\zeta} = 1$, $\gamma_{33} = \gamma_{\rho\rho} = 1$, and $\gamma_{\alpha\beta} = 0$ $(\alpha \neq \beta)$ was adopted. If there is no residual stress, $\kappa(B)$ with a metric tensor $\gamma_{\alpha\beta}$ is considered a stress-free reference configuration.

Local Stress-Free Configurations of Artery

The residual deformations of the common carotid artery[34] are shown in Fig. 1. Because the author did not determine the residual deformations of rabbit arteries[24] and could not find data of the local stress-

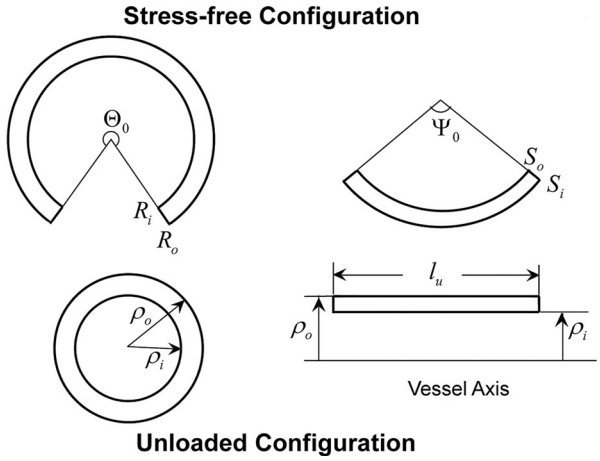

FIGURE 1. Schematic drawings of stress-free and unloaded configurations for an artery.[34] R_i and R_o denote the inner and outer radii of the stress-free sector, respectively, and Θ_0 the center angle of the sliced sector opened by a radial cut. S_i and S_o denote the radii of the inner and outer surfaces of the arc, respectively, and Ψ_0 the center angle of the arc of the axial strip of the unloaded vessel of the length l_u. The local stress-free configurations are ideally infinitesimally thin although the experimental local-stress free configurations have finite width. The inner and outer radii of the unloaded vessel are represented ρ_i and ρ_o, respectively. The length of l_u should be thought one between two marks along vessel axial direction because the full length of the specimen is subject to the end effect.

TABLE 1. Dimensions of sliced ring opened by a radial cut and axial strip curling to calculate distributions stretches and stresses through a rabbit arterial wall.

Local stress-free configurations
$R_i = 1.380$ mm, $R_0 = 1.617$ mm, $\Theta_0 = 201.2^*$ deg
$S_i = 4.732$ mm, $S_o = 4.495$ mm, $\Psi_0 = 124.2^*$ deg
Unloaded configuration
$\rho_i = 0.718$ mm, $\rho_o = 0.956$ mm, $l_u = 10.0$ mm

The symbols are defined in Fig. 1. (* porcine[34]).

free configurations for a rabbit artery in literature, a part of the data obtained for the porcine common carotid artery[34] was used in the present study. The estimated dimensions for the local stress-free configurations of the rabbit are summarized in Table 1. We assumed that the ring opened by a radial cut and the axial strip curling are stress free, i.e., those are the local stress-free configurations of the artery.

The nondiagonal components $\eta_{\alpha\beta}$ are zero because there are no residual shear deformations as shown in Fig. 1[34] whereas porcine coronary arteries have shown the shear residual deformation[35] as an axial strip became a helix. In the latter case, a Riemannian stress-free configuration needs nondiagonal components of the metric tensor.

From Fig. 1, the stretch ratios Λ_k $(k = \vartheta,\ \zeta,\ \rho)$ of the unloaded state with reference to the local stress-free configurations are provided as follows:

$$\begin{aligned}
\Lambda_\vartheta &= \frac{2\pi\rho}{\Theta_0 R(\rho)} \quad (R_i \le R \le R_o, \quad \rho_i \le \rho \le \rho_o) \\
\Lambda_\zeta &= \frac{l_u}{\Psi_0 S(\rho)} \quad (S_o \le S \le S_i) \\
\Lambda_\rho &= \frac{d\rho}{dR} = -\frac{d\rho}{dS} \quad (R - R_i = S_i - S)
\end{aligned} \tag{1}$$

It should be noted that the stretch ratio in the radial direction in the local stress-free configurations is common. The product of three principal stretch ratios is 1 based on the incompressibility of arterial wall,[2] i.e., we obtain the following equation:

$$\Lambda_\vartheta \Lambda_\zeta \Lambda_\rho = \frac{2\pi\rho}{\Theta_0 R}\frac{l_u}{\Psi_0 S}\frac{d\rho}{dR} = 1 \quad (S = S_i + R_i - R) \tag{2}$$

From the above equation, we obtain the following relation:

$$\rho = \sqrt{\frac{\Theta_0\Psi_0}{6\pi l_u}[-2R^3 + 3(R_i + S_i)R^2 - (R_i + 3S_i)R_i^2] + \rho_i^2} \tag{3}$$

where the angles are expressed in radian and we imposed a boundary condition $\rho_i = \rho(R_i)$. It is easily demonstrated that ρ increases as R increases for $R \in [R_i,\ R_o]$. Therefore, we can also obtain the inverse function $R = R(\rho)$ for $\rho \in [\rho_i,\ \rho_o]$.

Strain Energy Density Functions for Passive and Active Stresses

For the passive state of the artery, the following strain energy function[12] was adopted:

$$\begin{aligned}
W^{\text{passive}} &= \frac{\mu}{2}(I - 3) + \frac{k_1}{k_2}(\exp Q - 1), \\
Q &= k_2\left[(1 - \varsigma)(I - 3)^2 + \varsigma(K - 1)^2\right]
\end{aligned} \tag{4}$$

where μ and k_1 are constants with the dimension of energy density, and k_2 and $\varsigma \in [0,\ 1]$ denote nondimensional values, respectively. The invariants are expressed as follows:

$$I = g_{ij}\frac{\partial x^i}{\partial \xi^\alpha}\frac{\partial x^j}{\partial \xi^\beta}\eta^{\alpha\beta}, \quad K = \frac{1}{2}g_{ij}\frac{\partial x^i}{\partial \xi^\alpha}\frac{\partial x^j}{\partial \xi^\beta}(b_+^\alpha b_+^\beta + b_-^\alpha b_-^\beta) \tag{5}$$

where $b_\pm^\alpha$ denote components of unit vectors $b_\pm = (b_\pm^\vartheta,\ b_\pm^\zeta,\ b_\pm^\rho)$ in the Riemannian stress-free configuration, i.e., $\eta_{\alpha\beta}b_\pm^\alpha b_\pm^\beta = 1$ and their physical components were assumed $\bar{b}_+ = (\cos\varphi,\ \sin\varphi,\ 0)$ and $\bar{b}_- =$

$(\cos(\pi-\varphi),\ \sin(\pi-\varphi),\ 0)$ where φ and $\pi-\varphi$ denote mean angles of fibers against the circumferential direction with bimodal distribution[11] although φ was not determined by a histological observation. And $\eta^{\alpha\beta}$ are the reciprocal components of the metric tensor. Here, let λ_{i} $(i=\theta,\ z,\ r)$ denote the stretch ratio of a current configuration in each direction with reference to the Riemannian stress-free configuration:

$$\lambda_\theta = \Lambda_\vartheta\tilde{\lambda}_\theta,\quad \lambda_z = \Lambda_\zeta\tilde{\lambda}_z,\quad \lambda_r = \Lambda_\rho\tilde{\lambda}_r \tag{6}$$

where $\bar{\lambda}_i$ represent the stretch ratios of a current configuration χ with reference to the unloaded state. The first invariant may be simplified as $I=\lambda_\theta^2+\lambda_z^2+\lambda_r^2$ and K is simply expressed as $K=\lambda_\theta^2\cos^2\varphi+\lambda_z^2\sin^2\varphi$. Because the invariant K represents a fiber character, K must be larger than 1. If K became smaller than 1 in computing, it was set 1.

We assumed that the active stress is derived from the following strain energy function:

$$W^{\mathrm{active}} = \frac{C}{2}\tanh\left(g_{ij}\frac{\partial x^i}{\partial\xi^\alpha}\frac{\partial x^j}{\partial\xi^\beta}a^\alpha a^\beta - a\right) \tag{7}$$

where C has the energy density dimension and depends on the concentration of NA. In the experiments, NA was injected into an organ bath[25] at the concentration of 10^{-5} M to induce the maximal constriction of the smooth muscle cells. The symbols a^α denote contravariant components of a vector in the Riemannian stress-free configuration and the constant a is a scalar.

If there are no shear deformations, Eq. (7) may be expressed using physical components as follows:

$$W^{\mathrm{active}} = \frac{C}{2}\tanh(a_{\theta\theta}\lambda_\theta^2 + a_{zz}\lambda_z^2 + a_{rr}\lambda_r^2 - a) \tag{8}$$

where a_{ii} $(i=\theta,\ z,\ r)$ are the squares of physical components of the vector a^α. A function of the previous paper[24] was modified into the present one. The original strain energy function[24] is linear with the stretch ratios in the bracket as same as the function[14] but they cannot be extended to a general tensor form with shear strains because the linear form of strain energy function provides an asymmetric tensor for full covariant or contravariant components of the stress tensor. Therefore, we used Eq. (7) as a strain energy function providing the contractile stress of smooth muscle. Equation (8) provides a similar behavior as the functions[14,24] and it fits to the biaxial experimental data as shown in Fig. 2. Therefore, Eq. (8) similarly describes the smooth muscle character including anisotropic properties. However, it is not evident that Eq. (7) can well describe the smooth muscle tension under a shear deformation condition because any experiments have not been performed under shear strain condition.

The stress with the activated smooth muscle cells was assumed sum of the passive stress derived from W^{passive} and the active stress derived from W^{active}, i.e., we assumed that the stress under the activated condition may be derived from $W^{\mathrm{total}} = W^{\mathrm{passive}} + W^{\mathrm{active}}$.

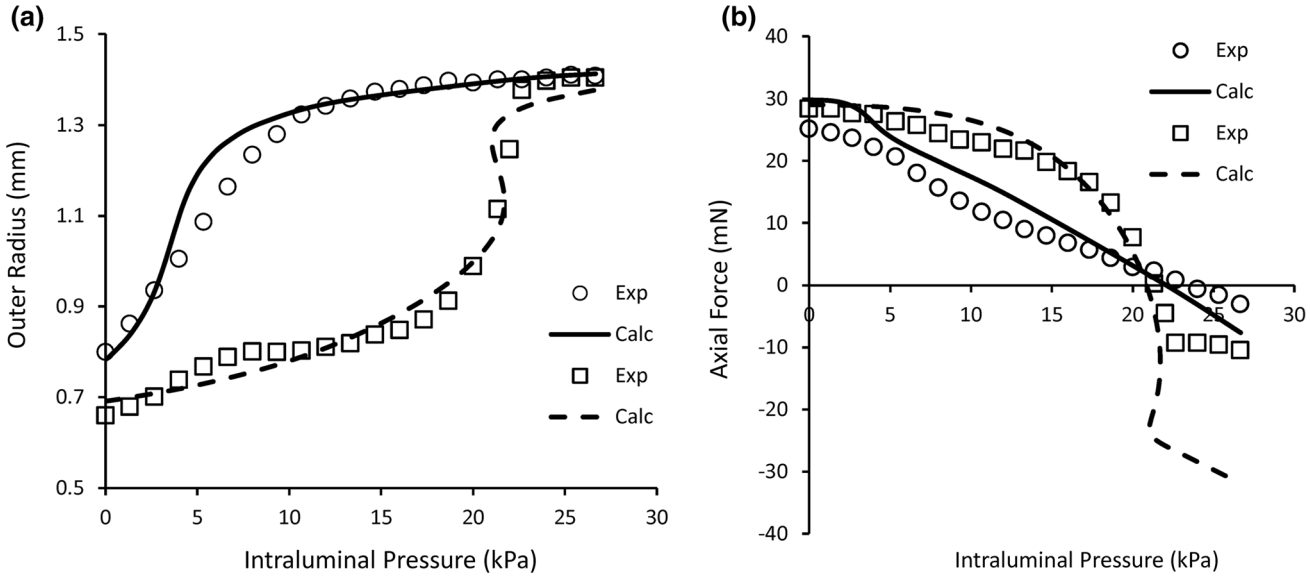

FIGURE 2. Outer radius vs. intraluminal pressure (a) and axial force vs. intraluminal pressure (b) relationships for passive and activated states. Axial stretch ratio is 1.5 with reference to the passive unloaded state. The passive experimental data are represented with (open circle) and the constricted experimental data with (open square). Solid and dashed curves are theoretically calculated ones using the parameters of Tables 1, 2, and 3 on Assumption-II.

The components of Cauchy stress t_{ij} are determined by the following equation for the compressible material:

$$t_{ij} = \frac{1}{J}\sqrt{\frac{\eta}{g}}\, g_{ik}\frac{\partial x^k}{\partial \xi^\alpha}\frac{\partial W}{\partial\left(\frac{\partial x^j}{\partial \xi^\alpha}\right)} \tag{9}$$

where $J = \det\left(\frac{\partial x^j}{\partial \xi^\alpha}\right)$, $\eta = \det(\eta_{\alpha\beta})$, and $g = \det(g_{ij})$. If material is incompressible, the constraint $J\sqrt{g} = \sqrt{\eta}$ is satisfied. Therefore, an undetermined Lagrange multiplier for the constraint of incompressibility of arterial wall H is introduced as follows:

$$t_{ij} = -Hg_{ij} + g_{ik}\frac{\partial x^k}{\partial \xi^\alpha}\frac{\partial W}{\partial\left(\frac{\partial x^j}{\partial \xi^\alpha}\right)} \tag{10}$$

where t_{ij} are covariant components of Cauchy stress. For the physical principal components of Cauchy stress, Eq. (10) is simplified as follows:

$$\sigma_{ii} = -H + \lambda_i\frac{\partial W}{\partial \lambda_i} \quad (i = \theta,\ z,\ r)\ \text{(not sum with } i) \tag{11}$$

for each strain energy density function.

We shall calculate the active stresses:

$$\sigma_{ii}^{\text{active}} = -H^{\text{active}} + Ca_{ii}\lambda_i^2\,\text{sech}^2\left(a_{\theta\theta}\lambda_\theta^2 + a_{zz}\lambda_{zz}^2 + a_{rr}\lambda_r^2 - a\right) \quad (i = \theta, z, r)\ \ \text{(not sum with } i) \tag{12}$$

Here, the principal active stress in the direction i is mainly determined by the term of $\text{sech}^2()$ approaching rapidly to 0 as λ_i decreases or increases from the value providing the maximum of $\text{sech}^2() = 1$. This may represent a typical response to the stretch of smooth muscle and the similar behavior of stresses depending on stretches in the published literature.[14,24]

Equilibrium Condition

For the incompressible thick-walled cylindrical artery under pressurized and axially stretched condition, a nontrivial equilibrium equation is provided as follows:

$$\frac{d\sigma_{rr}}{dr} + \frac{\sigma_{rr} - \sigma_{\theta\theta}}{r} = 0 \quad (\sigma_{rr}(r_i) = -P_i,\ \sigma_{rr}(r_o) = -P_o = 0) \tag{13}$$

where σ_{ii} $(i = \theta,\ z,\ r)$ are physical principal components of Cauchy stress. From Eq. (13) with the boundary conditions, the intraluminal pressure may be calculated as follows:

$$P_i = \int_{r_i}^{r_o}\frac{\sigma_{\theta\theta} - \sigma_{rr}}{r}dr = \int_{r_i}^{r_o}\left(\lambda_\theta\frac{\partial W}{\partial \lambda_\theta} - \lambda_r\frac{\partial W}{\partial \lambda_r}\right)\frac{dr}{r} \tag{14}$$

The axial force was calculated as follows:

$$\begin{aligned} F_z &= -\pi r_i^2 P_i + 2\pi\int_{r_i}^{r_o}\sigma_{zz}rdr \\ &= 2\pi\int_{r_i}^{r_o}[\sigma_{zz} - (\sigma_{\theta\theta} + \sigma_{rr})/2]rdr \\ &= 2\pi\int_{r_i}^{r_o}\left[\lambda_z\frac{\partial W}{\partial \lambda_z} - \frac{1}{2}\left(\lambda_\theta\frac{\partial W}{\partial \lambda_\theta} + \lambda_r\frac{\partial W}{\partial \lambda_r}\right)\right]rdr \end{aligned} \tag{15}$$

Here, the first line is definition of external axial force. We shall prove the following relationship:

$$r_o^2\sigma_{rr}(r_o) - r_i^2\sigma_{rr}(r_i) = \int_{r_i}^{r_o}(\sigma_{\theta\theta} + \sigma_{rr})rdr \tag{16}$$

Using integration by parts and Eq. (13), we obtain:

$$\begin{aligned} \int_{r_i}^{r_o}2r\sigma_{rr}(r)dr &= [r^2\sigma_{rr}(r)]_{r_i}^{r_o} - \int_{r_i}^{r_o}r^2\frac{d\sigma_{rr}(r)}{dr}dr \\ &= r_o^2\sigma_{rr}(r_o) - r_i^2\sigma_{rr}(r_i) - \int_{r_i}^{r_o}r^2\frac{\sigma_{\theta\theta} - \sigma_{rr}}{r}dr \end{aligned} \tag{17}$$

From the boundary conditions of Eq. (13), the second line of Eq. (15) is obtained.

In Fig. 2, the theoretical curves under the activated condition have a small local peak of the pressure. Therefore, the curves become multivalued functions with the independent argument of pressure. The curves are calculated as functions of the outer radius r_o with Eqs. (14) and (15). They are an ordinary function from the outer radius to the pressure in Fig. 2a and that from the outer radius to the axial force in Fig. 2b. For the experimental results these problems did not occur.

Parameter Estimation by Nonlinear Regression

Material parameters of each strain energy function were determined by a least squares method using MATLAB (*fminsearch*: Nelder-Mead method)[19] with results calculated by Eqs. (14) and (15). First the material parameters of the passive strain energy function were determined for the passive experimental data. Then the material parameters of the active strain energy function were determined for the experimental data subtracted by the results calculated by the passive strain energy function determined at first. Weights for the differences between the calculated and experimental values were assigned to provide the mean stresses. The sum e of squares of the weighted residues was

minimized by searching the material parameters of the strain energy functions as follows:

$$e = \sum_{k=1}^{N} \left\{ [r_i/(r_0 - r_i)]^{\exp} \left(P_i^{calc} - P_i^{\exp} \right) \right\}_k^2 + \sum_{k=1}^{N} \left\{ \left(F_z^{calc} - F_z^{\exp} \right) / \left[\pi \left(r_o^2 - r_i^2 \right) \right]^{\exp} \right\}_k^2 \quad (18)$$

where the difference between the calculated result and experimental data is at the k-th radius and N denotes a number of total data points used for the estimation of the material parameters.

RESULTS

Because at the intraluminal pressures equal or higher than 170 mmHg the outer diameters increased slightly as pressures greatly increased, the diameter data were affected by the noise of the signals of CCD camera. In some cases, the diameter decreased as the pressure increased. Therefore, the difference between the passive pressure and activated pressure data at the same diameter could not be determined. Therefore, we excluded data points at the top 4 pressures of 170, 180, 190, and 200 mmHg (100 mmHg = 13.332 kPa) and added the data point at a pressure of 165 mmHg. This procedure did not fit the theoretical results for the top 4 pressure data compared to using all the data, but by removing the top 4 pressure data, the conformity has been greatly improved in the middle range. The experimental data and theoretical results are shown in Fig. 2. Criterion of the fitting of the theoretical result to the experimental data was adopted as the following value based on Eq. (18):

$$\mathrm{SD} = \sqrt{e/(2N)} \quad (19)$$

Appling this to determine the goodness of fitting, if all data (0–200 mmHg) were used: SD = 10.25 kPa and if excluding top 4 data (0–165 mmHg): SD = 6.76 kPa. Thus, the removing top 4 data yields better fitting.

The theoretical results for pressure and axial force as functions of radius on the assumptions of only the sliced ring opened by a radial cut (Assumption-I), and

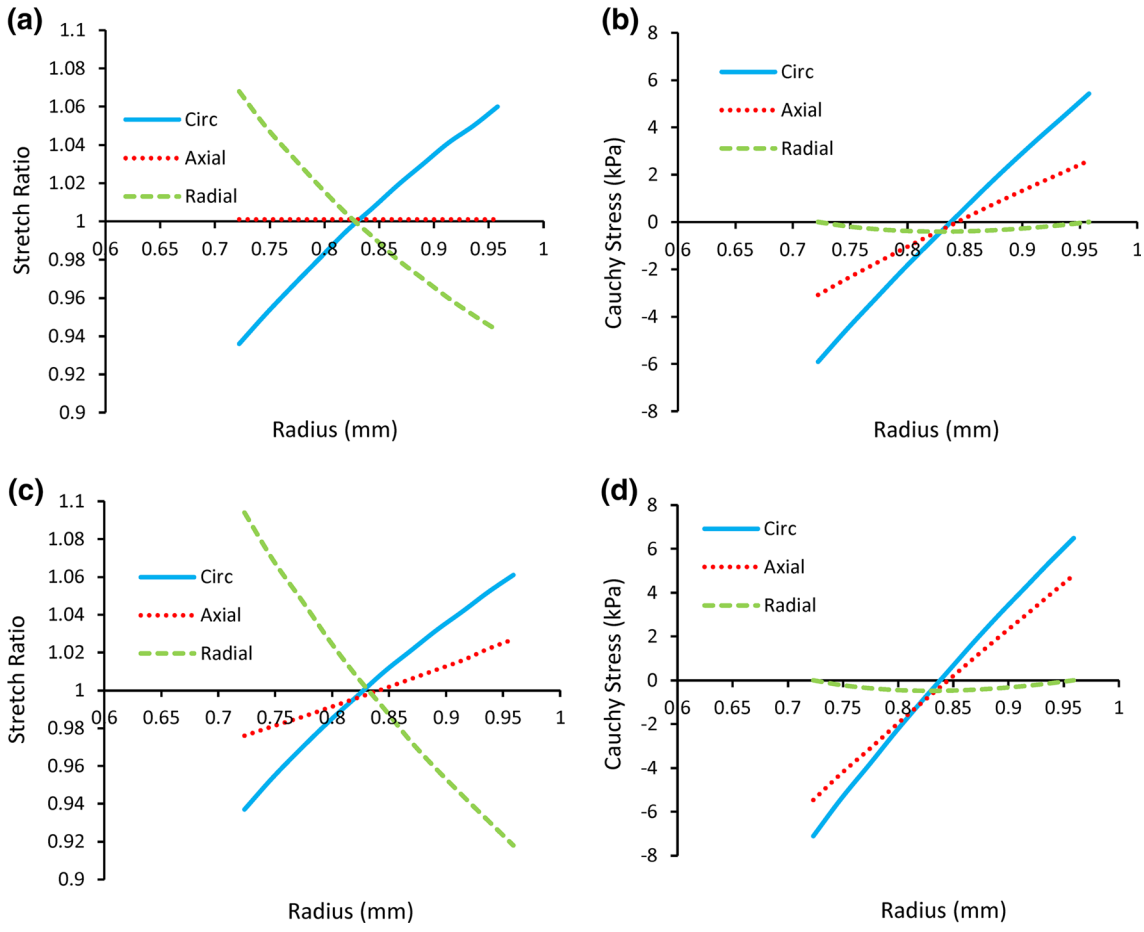

FIGURE 3. Distributions of residual stretch ratios and stresses in the passive state based on Assumption-I (a, b) and on Assumption-II (c, d).

both the sliced ring opened and axial strip curling (Assumption-II) were almost the same. Therefore, we show only those calculated on Assumption-II (Fig. 2). The theoretical axial force under vasoactive condition in Fig. 2[24] was not well fitted to the experimental data at the top 4 pressures whereas a good coincidence was obtained in the low and middle ranges to the exclusion of the top 4 pressures in the fitting. In the following, we shall compute both the distributions of stretch ratio and stress using the material parameters determined without the data at the top 4 pressures in the vasoconstrictive experiment, i.e., we chose the coincidence

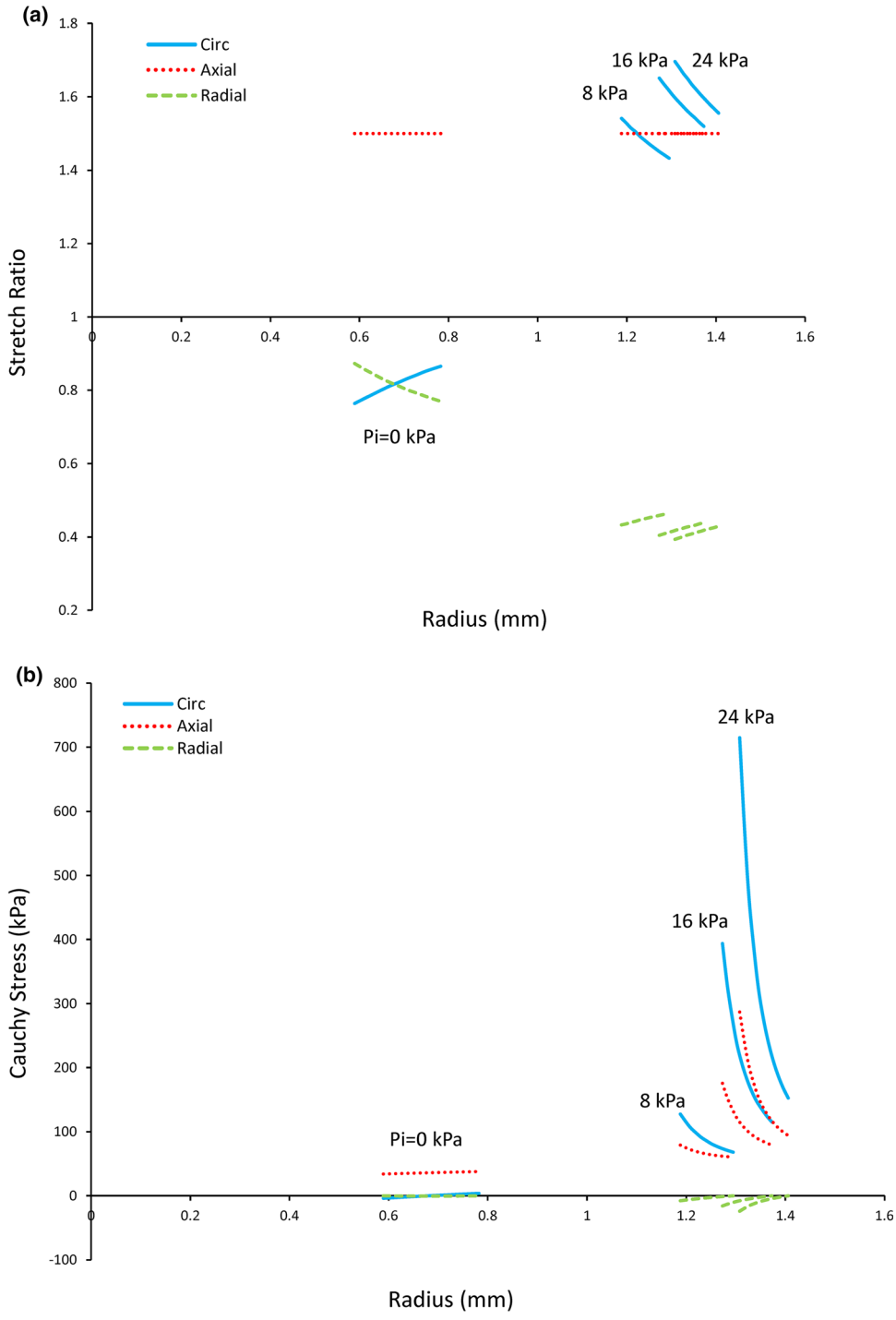

FIGURE 4. Distributions of stretch ratios in passive states at intraluminal pressures of 0, 8, 16, and 24 kPa are shown in (a). Axial stretch ratio is 1.5 with reference to the passive unloaded state. Those of stresses are shown in (b). The graphs are based on Assumption-I.

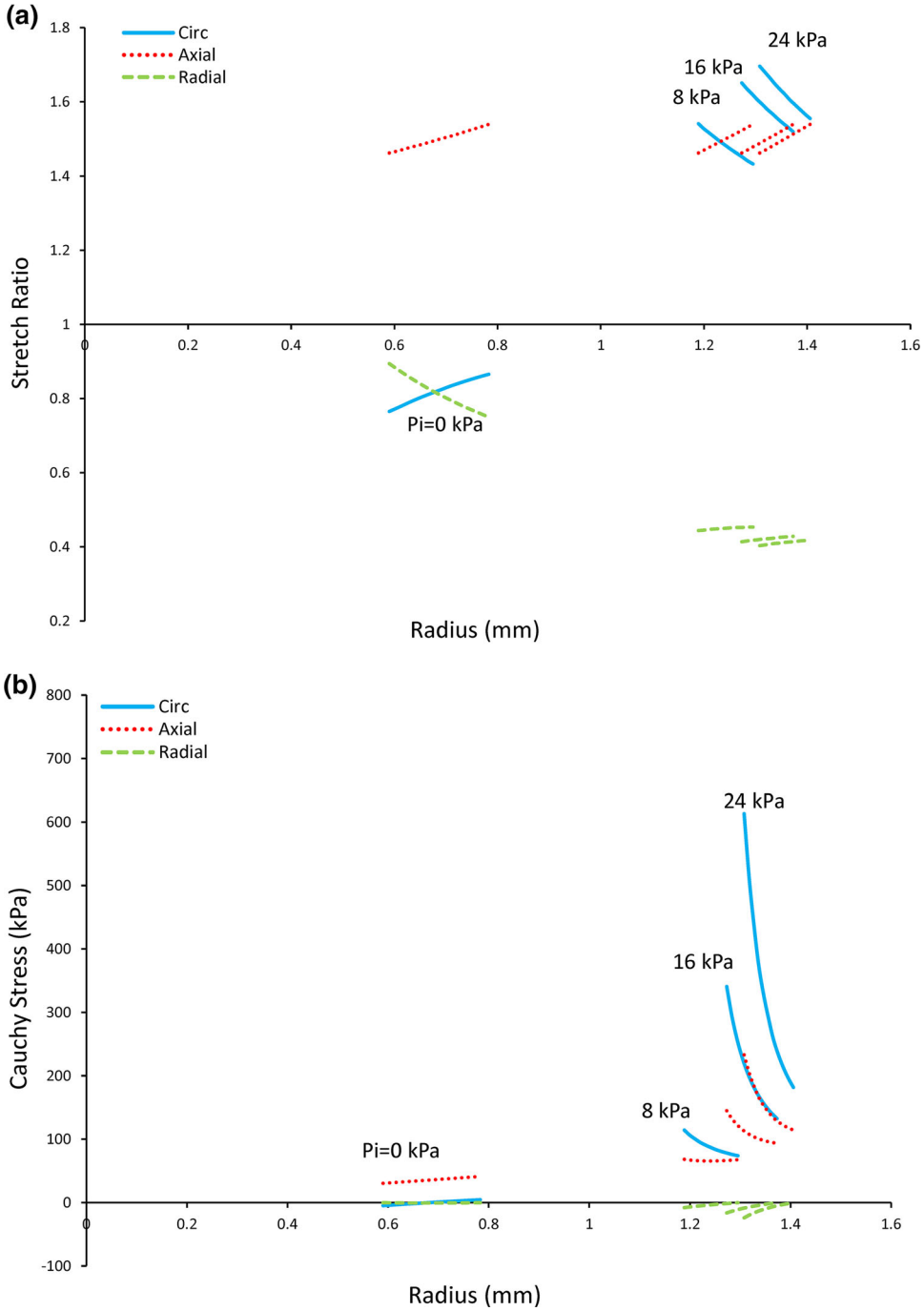

FIGURE 5. Distributions of stretch ratios in the passive state at intraluminal pressures of 0, 8, 16, and 24 kPa are shown in (a). Axial stretch ratio is 1.5 with reference to the passive unloaded state. Those of stresses are shown in (b). The graphs are based on Assumption-II.

between theoretical and experimental results in the low and middle ranges of pressures at the expense of the coincidence in the top range because we did not use the results in this range to analyze the stretch ratios and stresses in the vasoconstrictive state of the artery. The material parameters of the strain energy density functions on Assumption-I and II are shown in Tables 2 and 3.

We show distributions of residual stretch ratio and stress under the passive condition on Assumption-I and II through the wall thickness in Fig. 3. The residual axial stretch ratio is constant and close to 1 on

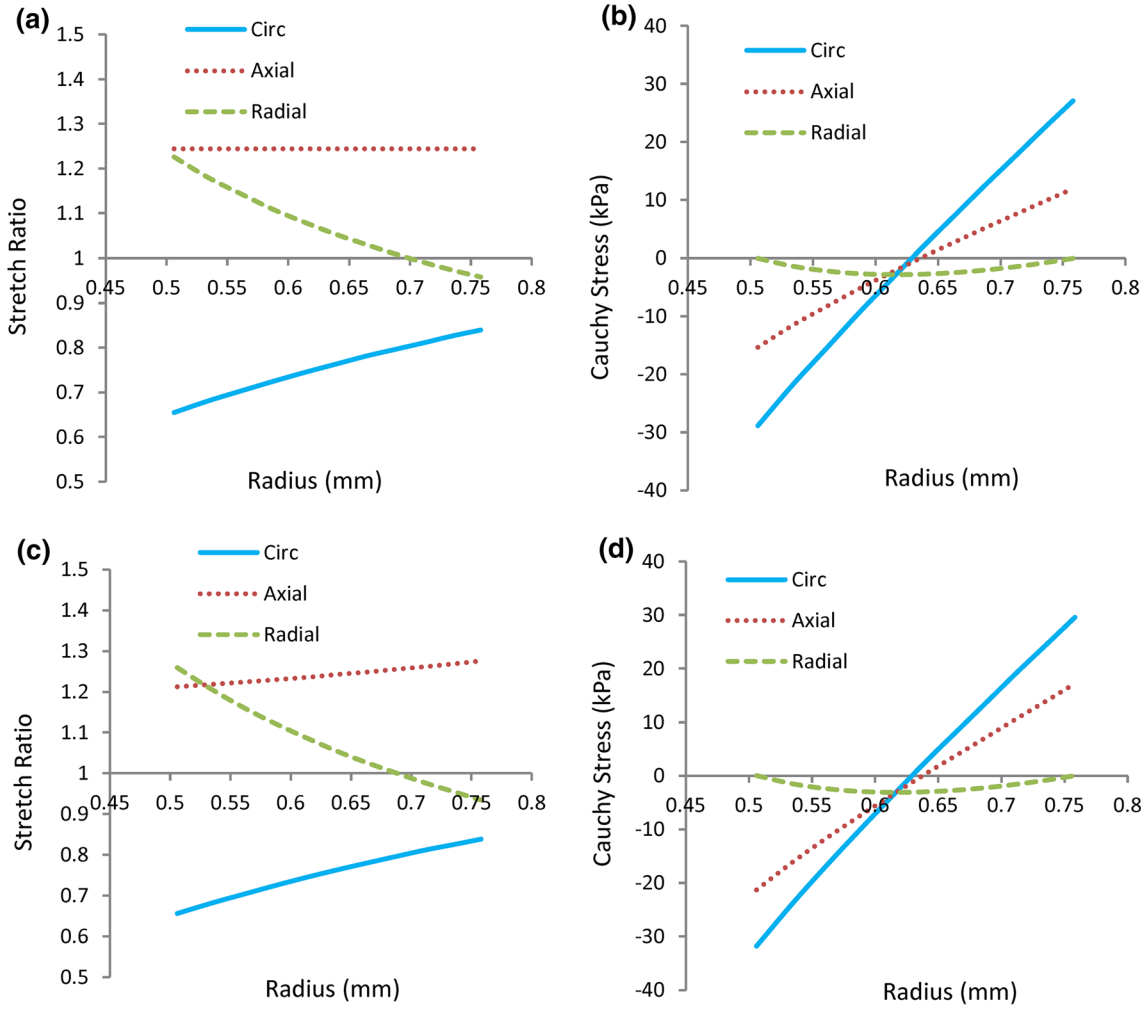

FIGURE 6. Distributions of residual stretch ratios and stresses in the active state based on Assumption-I (a, b) and on Assumption-II (c, d).

Assumption-I (Fig. 3a) whereas it increases from the inner surface to the outer surface on Assumption-II (Fig. 3c). However, residual stresses are similar distributions on Assumption-I and II (Figs. 3b and 3d).

Distributions of stretch ratio and stress at intraluminal pressures of 0, 8, 16, and 24 kPa and at an axial stretch ratio 1.5 with reference to the unloaded state on Assumption-I are shown in Figs. 4a and 4b, respectively. Those on Assumption-II are shown in Figs. 5a and 5b. The differences between the results calculated on Assumption-I and II were small compared with the results[34] although those were for the porcine common carotid artery.

The passive stretch ratios and stresses greatly decreased from the inner surface to the outer surface. These are different from results of canine common carotid arteries on uniform strain hypothesis.[25] The author thinks that the uniform strain hypothesis might not well work under general conditions even in healthy animals. The opening angle depends on site of aorta in rat.[8,9] In the porcine common carotid arteries, the opening angles of arcs of axial strip may also vary depending on position.[34]

For the unloaded state, the results activated with NA are shown in Fig. 6 on Assumption-I and II. The circumferential stretch ratios are smaller than 1 and the axial stretch ratios are larger than 1 on the both assumptions. The residual stresses become large compared with the passive state and their distributions are similar on Assumption-I and II.

Distributions of stretch ratio and stress in the activated state at the intraluminal pressures of 0, 8, 16, and 24 kPa at the axial stretch ratio 1.5 with reference to the passive unloaded state are shown in Figs. 7a and 7b on Assumption-I, respectively. Those on Assumption-II are shown in Figs. 8a and 8b. The circumferential and axial stresses in the active state are low compared with the passive state. The circumferential

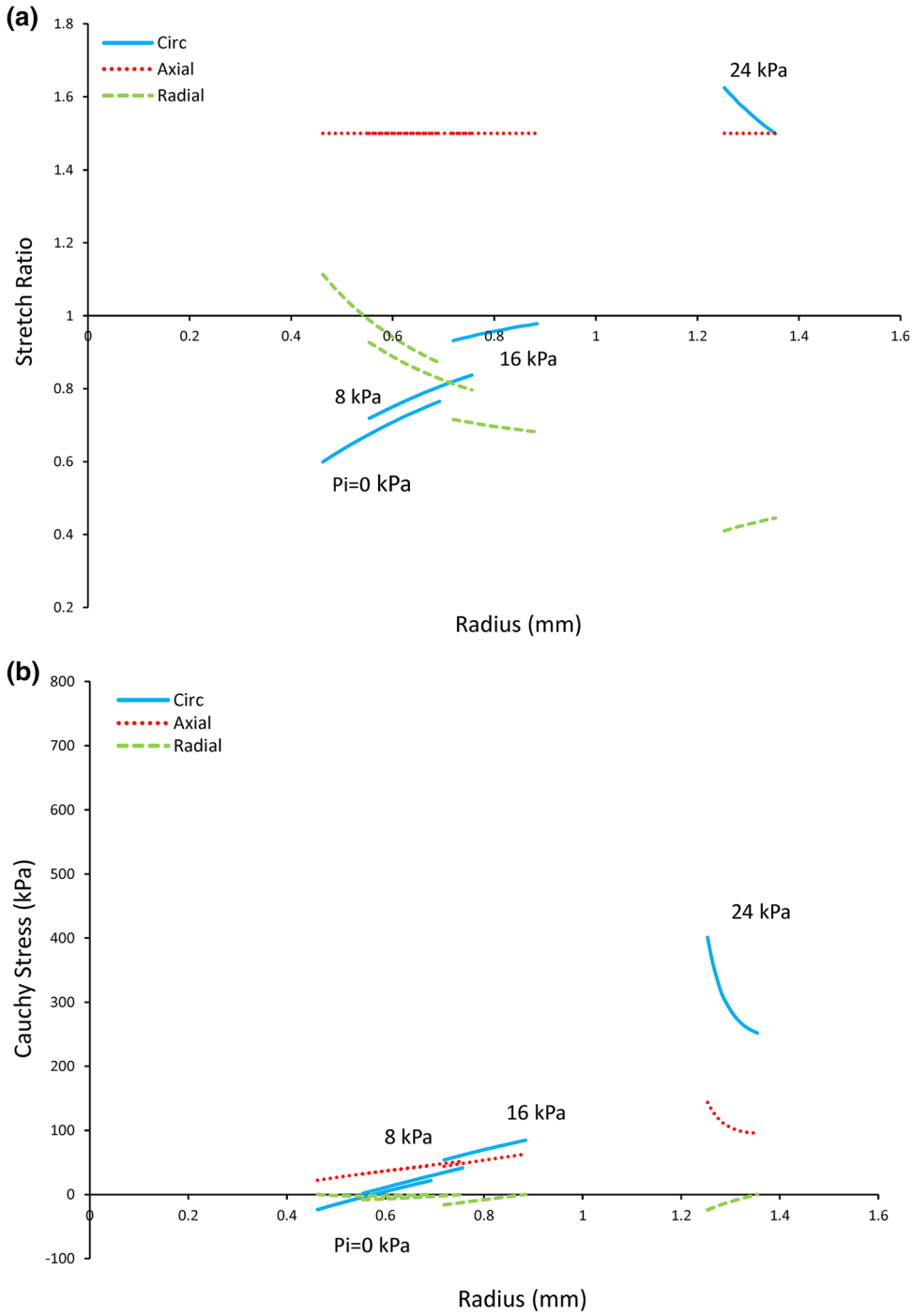

FIGURE 7. Distributions of stretch ratios in active state at intraluminal pressures of 0, 8, 16, and 24 kPa are shown in (a). Axial stretch ratio is 1.5 with reference to the passive unloaded state. Those of stresses are shown in (b). The graphs are based on Assumption-I.

and axial stresses with activated smooth muscle at the intraluminal pressure 16 kPa and the axial stretch ratio 1.5 with reference to the unloaded vessel decreased by 3.5 and 13.8% at the inner surface with considering the axial residual strain, respectively.

DISCUSSION

Axial Residual Strain

In the present study, the residual axial stretch ratio had small difference from 1 compared with the other

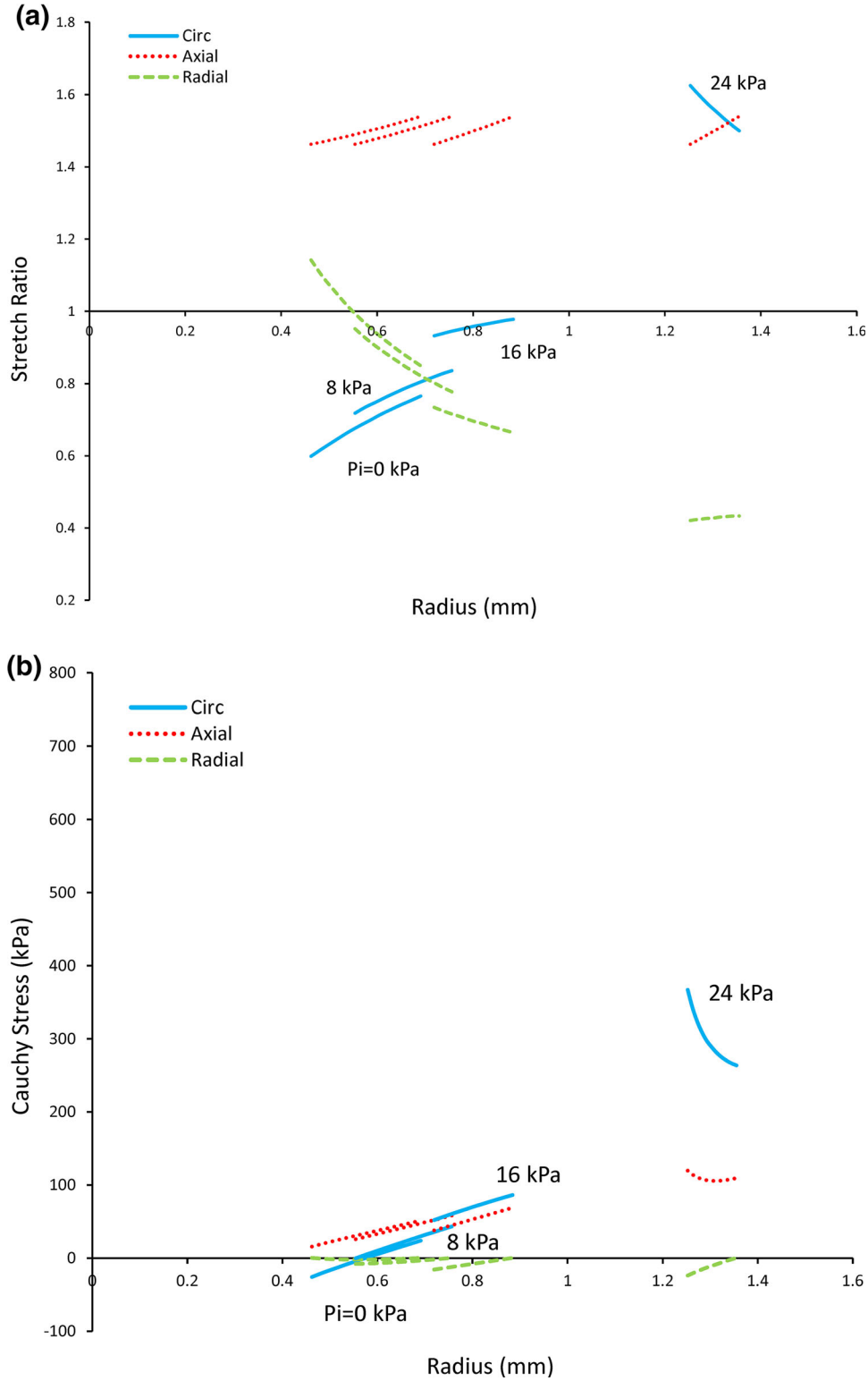

FIGURE 8. Distributions of stretch ratios in active state at intraluminal pressures of 0, 8, 16, and 24 kPa are shown in (a). Axial stretch ratio is 1.5 with reference to the passive unloaded state. Those of stresses are shown in (b). The graphs are based on Assumption-II.

example.[34] Therefore, there appeared small differences between the estimated material parameters included in the strain energy density functions based on Assumption-I and II as shown in Tables 2 and 3. The difference between the calculated results of distributions of stretch ratio and stress on Assumption-I and II was also small under the physiologically loaded condition. There is, however, a possibility that circumferential and axial residual strains are large compared with the present study because those provided were not experimentally determined with the present specimen. The author thinks that the difference between the rabbit and porcine common carotid arteries seems to be a quantitative one and they are qualitatively similar mechanical properties in the passive and activated states.

Reference Configuration for Active Stress–Stretch Relationship

A reference state of an active condition is generally different from the stress-free state of the passive one. Therefore, the stress-free state in Fig. 1 should be modified for the active state. We chose, however, the stress-free state for the passive configuration as a reference state to compute the activated stress because there is not the stress-free state of the active stress due to the form of constitutive law of the active stress except for the isotropic case (Eq. (12)). The active constitutive law was assumed to be valid in the form of the present study with reference to the passive reference configuration, i.e., a_{ii} $(i = \theta,\ z,\ r)$ in Eq. (8) are constant even if they are determined with the stretch ratios of a current configuration with reference to the passive stress-free state.

TABLE 2. Material parameters of the strain energy density function for the passive state of the artery based on only sliced ring opened by a radial cut (Assumption-I) and both sliced ring opened by a radial cut and axial strip curling (Assumption-II).

	μ (kPa)	k_1 (kPa)	k_2	ς	φ (°)
I	22.390	0.611	1.257	0.829	29.883
II	22.347	0.595	1.298	0.836	30.303

TABLE 3. Material parameters of the strain energy density function which provides the active stresses of the artery on the Assumption-I and II.

	C (kPa)	$a_{\theta\theta}$	a_{zz}	a_{rr}	a
I	129.177	0.773	0.136	0.253	1.477
II	128.830	0.774	0.135	0.248	1.478

Stress Relaxation of Axial Strip with Vasoconstrictor

In the activated state with NA, the magnitude of residual strains and stresses was large compared with the passive state as shown in Fig. 6. The circumferential residual stretch ratio decreased and the axial residual stretch increased significantly compared with those in the passive state. The residual stresses were also large compared with those in the passive state. However, the differences between results on Assumption-I and II were small because the axial residual strain calculated on Assumption-II was little different from that calculated on Assumption-I. Anyway, these results explained the experimental results for canine strips subdivided in various directions,[20] i.e., the experiment showed that the strip specimen in the circumferential direction provided tension and the axial strip did dilation with vasoconstrictive agents, including NA. This fact is consistent with the present theory. We analyzed in details for the activated tensions on the rabbit circumferential and axial strips. A strip sectioned in the circumferential direction under conditions of $\lambda_\theta = 1.3$, and $\sigma_{zz} = \sigma_{rr} = 0$ yields $\sigma_{\theta\theta} = 22.0$ kPa in the passive state using material parameters in Table 2 (II), and in the activated state $\sigma_{\theta\theta} = 170.2$ kPa using the material parameters for the passive state and the active strain energy density function in Tables 2 and 3 (II). This means that the strip generates the active circumferential stress 148.2 kPa. On the other hand, an axial strip under conditions $\lambda_z = 1.3$, and $\sigma_{\theta\theta} = \sigma_{rr} = 0$ yields $\sigma_{zz} = 20.7$ kPa in the passive state and $\sigma_{zz} = 8.5$ kPa in the activated state. This implies that the axial tension decreases by 12.2 kPa, i.e., the dilation occurred with NA. All results were obtained using the material parameters estimated on Assumption II and the stretch ratio of strip follows the experimental condition of the study.[20] The material parameters included in the strain energy density functions have small differences between Assumption-I and II. The almost same results may be yielded on both the assumptions. In any way, we can explain the relaxation with the vasoconstrictor in the axial strip with the present strain energy density functions.

Limitations of the Present Study and Future Objectives

The present study assumes the homogeneous one-layer straight tube with cylindrical symmetry. And the other limitation is that the experiments have been performed without shear strains. It is needed to validate Eq. (7) with shear strains.

The other possible direction is the distributed fibers model for passive artery. Holzapfel and his coworkers, and Kassab and his coworkers have progressed in this direction. The Riemannian stress-free configuration may be useful for their studies.

Next objective will be chemomechanical contractile model. The chemomechanical model may provide a time dependent character while the active tension is developing.

The Riemannian stress-free configuration has interesting applications to the remodeling of growth[36] and the collapse[7] in arteries because the change of stress distributions with the residual stresses may have effect on these phenomena.

CONFLICT OF INTEREST

This work was conducted by a now retired researcher of National Cerebral and Cardiovascular Center Research Institute in Osaka without support from any funding organization. The author declares that he has no conflict of interest.

ETHICAL APPROVAL

All care and use of laboratory animals followed JALAS (Japanese Association for Laboratory Animal Science) Guidelines on Animal Experimentation (in Japanese).[15] The experiments were performed by the author in 1992 at National Cardiovascular Center Research Institute (National Cerebral and Cardiovascular Center Research Institute since 2010).

APPENDIX

In the present analysis, the Riemannian stress-free configuration[23,27,28] was used for the reference state. This is not the necessary choice to analyze the strains and stresses in the artery because the local stress-free configurations are also available. It may be decided by using the Riemann–Christoffel tensor whether the Euclidean global stress-free configuration exists or not. If the axial strip sectioned from the vessel wall does not curl, there exists the global Euclidean stress-free configuration, i.e., a straight tube with an axial slit is that.[23]

The covariant components of the Riemann-Christoffel tensor[21] for the stress-free configuration are expressed as follows:

$$R_{\alpha\beta\mu\nu} = \frac{1}{2}\left(\frac{\partial^2\eta_{\alpha\nu}}{\partial\xi^\beta\partial\xi^\mu} + \frac{\partial^2\eta_{\beta\mu}}{\partial\xi^\alpha\partial\xi^\nu} - \frac{\partial^2\eta_{\alpha\mu}}{\partial\xi^\beta\partial\xi^\nu} - \frac{\partial^2\eta_{\beta\nu}}{\partial\xi^\alpha\partial\xi^\mu}\right) + \eta^{\delta\varepsilon}(\Gamma_{\delta\alpha\nu}\Gamma_{\varepsilon\beta\mu} - \Gamma_{\delta\alpha\mu}\Gamma_{\varepsilon\beta\nu}) \tag{20}$$

where $\eta^{\delta\varepsilon}$ represent the reciprocal components of the metric tensor. In the three-dimensional space, there exist distinct covariant components of the Riemann–Christoffel tensor $R_{1212} = R_{\vartheta\zeta\vartheta\zeta}$, $R_{1313} = R_{\vartheta\rho\vartheta\rho}$, $R_{2323} = R_{\zeta\rho\zeta\rho}$, $R_{1213} = R_{\vartheta\zeta\vartheta\rho}$, $R_{2123} = R_{\zeta\vartheta\zeta\rho}$.[21] Therefore, we must check these components to know whether the Riemannian stress-free configuration is Euclidean or not. If there is a global Euclidean stress-free configuration, all components vanish everywhere.

The length s of a curve $\xi^\alpha = \xi^\alpha(\tau)$ $(\alpha = 1, 2, 3)$ in the Riemannian stress-free configuration is defined as follows:

$$s = \int_{\tau_1}^{\tau_2} \sqrt{\eta_{\alpha\beta}\frac{d\xi^\alpha}{d\tau}\frac{d\xi^\beta}{d\tau}}\,d\tau \tag{21}$$

Here, $\eta_{\alpha\beta}$ are functions of only $\rho \in [\rho_i,\ \rho_o]$ in the present case. The length of $\Theta_0 R$ with the circular arc is provided as follows (see Fig. 1 and Eq. (1)):

$$\Theta_0 R = \int_0^{2\pi} \sqrt{\eta_{\vartheta\vartheta}}\,d\theta = 2\pi\sqrt{\eta_{\vartheta\vartheta}} \tag{22}$$

In the same way, we obtain as follows:

$$\begin{aligned} \Psi_0 S &= \int_0^{l_u} \sqrt{\eta_{\zeta\zeta}}\,d\zeta = \sqrt{\eta_{\zeta\zeta}}\,l_u, \\ R - R_i = S_i - S &= \int_{\rho_i}^{\rho} \sqrt{\eta_{\rho\rho}(\rho')}\;d\rho' \end{aligned} \tag{23}$$

The components of the metric tensor for the Riemannian stress-free configuration are provided from Eqs. (23) and (24):

$$\begin{aligned} \eta_{\vartheta\vartheta} &= \left(\frac{\Theta_0 R}{2\pi}\right)^2,\ \eta_{\zeta\zeta} = \left(\frac{\Psi_0 S}{l_u}\right)^2, \\ \eta_{\rho\rho} &= \left(\frac{dR}{d\rho}\right)^2 = \left(\frac{dS}{d\rho}\right)^2, \\ \eta_{\alpha\beta} &= 0 \quad (\alpha \neq \beta) \end{aligned} \tag{24}$$

Is the coordinate system for the Riemannian stress-free configuration $\langle \xi^\alpha;\ \eta_{\alpha\beta} \rangle$ Euclidean? We calculated six components of the Riemann–Christoffel tensor. The result was as follows:

$$R_{\vartheta\zeta\vartheta\zeta} = \left(\frac{\Theta_0\Psi_0}{2\pi l_u}\right)^2 RS > 0 \tag{25}$$

The other five components were equal to zero. Therefore, the Riemannian stress-free configuration $\kappa(B)$ with the metric tensor $\eta_{\alpha\beta}$ is non-Euclidean although the other five components vanish. This means that there is no global Euclidean stress-free configuration. If there is no curling of axial strip, Eq. (25) becomes zero. It is evident that $R_{\vartheta\zeta\vartheta\zeta}$ approaches to zero because Ψ_0 approaches to zero, S infinitely increases, and the product $\Psi_0 S$ is almost maintaining

l_u. In this case there is a global Euclidean stress-free configuration, i.e., a tubular segment with a slit may be the stress-free state.

REFERENCES

[1]Böl, M., and A. Schmitz. A coupled chemomechanical model for smooth muscle contraction. In: Computer Models in Biomechanics. From Nano to Macro, edited by G. A. Holzapfel, and E. Kuhl. Dordrecht: Springer, 2013, pp. 63–75.

[2]Carew, T. E., R. N. Vaishnav, and D. J. Patel. Compressibility of the arterial wall. *Circ. Res.* 23:61–68, 1968.

[3]Chuong, C. J., and Y. C. Fung. On residual stresses in arteries. *J. Biomech. Eng.* 108:189–192, 1986.

[4]Cox, R. H. Mechanics of canine iliac artery smooth muscle in vitro. *Am. J. Physiol.* 230:462–470, 1976.

[5]Dobrin, P. B. Influence of initial length on length-tension relationships of vascular smooth muscle. *Am. J. Physiol.* 225:664–670, 1973.

[6]Dobrin, P. B., and A. A. Rovick. Influence of smooth muscle on contractile mechanics and elasticity. *Am. J Physiol.* 217:1644–1651, 1969.

[7]Fatemifar, F., and H. C. Han. Effect of axial stretch on lumen collapse of arteries. *J. Biomec. Eng.* 138:124503, 2016.

[8]Fung, Y. C. Biomechanics: Motion, Flow, Stress, and Growth. New York: Springer, 1998.

[9]Fung, Y. C., and S. Q. Liu. Change of residual strains in arteries due to hypertrophy caused by aortic constriction. *Circ. Res.* 65:1340–1349, 1989.

[10]Holzapfel, G. A., and R. W. Ogden. Modelling the layer-specific three-dimensional residual stresses in arteries with an application to the human aorta. *J. R. Soc. Interface* 7:787–799, 2010.

[11]Holzapfel, G. A., T. C. Gasser, and R. W. Ogden. A new constitutive framework for arterial wall mechanics and comparative study of material models. *J. Elast.* 61:1–48, 2000.

[12]Holzapfel, G. A., G. Sommer, C. T. Gasser, and P. Regitnig. Determination of layer-specific mechanical properties with nonatherosclerotic intimal thickening and related constitutive modeling. *Am. J. Physiol. Heart Circ. Physiol.* 289:H2048–H2058, 2005.

[13]Holzapfel, G. A., G. Sommer, M. Auer, P. Regitnig, and R. W. Ogden. Layer-specific three-dimensional residual deformations of human aortas with non-atherosclerotic intimal thickening. *Ann. Biomed. Eng.* 35:530–545, 2007.

[14]Huo, Y., Y. Cheng, X. Zhao, X. Liu, and G. S. Kassab. Biaxial vasoactivity of porcine coronary artery. *Am. J. Physiol. Heart Circ. Physiol.* 302:H2058–H2063, 2012.

[15]JALAS (Japanese Association for Laboratory Animal Science). Guidelines on animal experimentation (in Japanese). *Exp. Anim.* 36:285–288, 1987.

[16]Lu, X., J. Yang, J. B. Zhao, H. Gregersen, and G. S. Kassab. Shear modulus of porcine coronary artery: Contribution of media and adventitia. *Am. J. Physiol. Heart Circ. Physiol.* 285:H1966–H1975, 2003.

[17]Lu, X., A. Pandit, and G. S. Kassab. Biaxial incremental homeostatic elastic moduli of coronary artery: Two-layer model. *Am. J. Physiol. Heart Circ. Physiol.* 287:H1663–H1669, 2004.

[18]Murtada, S. A., M. Kroon, and G. A. Holzapfel. A calcium-driven mechanochemical model for prediction of force generation in smooth muscle. *Biomech. Model Mechanobiol.* 9:749–762, 2010.

[19]Nelder, J. A., and R. Mead. A simplex method for function minimization. *Comput J.* 7:308–313, 1965.

[20]Ohhashi, T., and T. Azuma. Paradoxical relaxation of arterial strips induced by vasoconstrictive agents. *J. Vasc. Res. (Blood Vessels)* 17:16–26, 1980.

[21]Sokolnikoff, I. S. Tensor Analysis: Theory and applications to geometry and mechanics of continua (2nd ed.). New York: Wiley, pp. 89–91, 1964; ((pp. 326–327)).

[22]Stålhand, J. A., A. Klarbring, and G. A. Holzapfel. Smooth muscle contraction: Mechanochemical formulation for homogeneous finite strains. *Prog. Biophys. Mol. Biol.* 96:465–481, 2008.

[23]Takamizawa, K. Stress-free configuration of a thick-walled cylindrical model of the artery: An application of Riemann geometry to the biomechanics of soft tissues. *J Appl Mech.* 58:840–842, 1991.

[24]Takamizawa, K. Biaxial contractile mechanics of common carotid arteries of rabbit. *J. Biomech. Eng.* 137:031010, 2015.

[25]Takamizawa, K., and K. Hayashi. Strain energy density function and uniform strain hypothesis for arterial mechanics. *J. Biomech.* 20:7–17, 1987.

[26]Takamizawa, K., and K. Hayashi. Uniform strain hypothesis and thin-walled theory in arterial mechanics. *Biorheol* 25:555–565, 1988.

[27]Takamizawa, K., and T. Matsuda. Kinematics for bodies undergoing residual stress and its applications to the left ventricle. *J. Appl. Mech.* 57:321–329, 1990.

[28]Takamizawa, K., and Y. Nakayama. Non-Euclidean stress-free configuration of arteries accounting for curl of axial strips sectioned from vessels. *J. Biomech. Eng.* 135:114505, 2013.

[29]Takamizawa, K., K. Hayashi, and T. Matsuda. Isometric biaxial tension of smooth muscle in isolated cylindrical segments of rabbit arteries. *Am. J. Physiol. Heart Circ. Physiol.* 32:H30–H34, 1992.

[30]Truesdell, C., and W. Noll. The nonlinear field theory of mechanics. In: Encyclopedia of Physics, Vol. III/3, edited by S. Flügge. Berlin: Springer, 1965, pp. 51–52.

[31]Vaishnav, R. N., and J. Vossoughi. Estimation of residual strains in aortic segments. In: Biomedical Engineering 2: Recent Developments, edited by W. Hall. Proceedings of the Second Southern Biomedical Engineering, Amsterdam: Elsevier, 1983, pp. 330–333.

[32]Vaishnav, R. N., and J. Vossoughi. Residual stress and strain in aortic segments. *J. Biomech.* 20:235–239, 1987.

[33]Wagner, H. P., and J. D. Humphrey. Differential passive and active biaxial mechanical behaviors of muscular and elastic arteries: Basilar versus common carotid. *J. Biomech. Eng.* 133:051009, 2011.

[34]Wang, R., and R. L. Gleason. A mechanical analysis of conduit arteries accounting for longitudinal residual strains. *Ann. Biomed. Eng.* 38:1377–1387, 2010.

[35]Wang, R., and R. L. Gleason. Residual shear deformations in the coronary artery. *J. Biomech. Eng.* 136:061004, 2014.

[36]Yavari, A. A geometric theory of growth mechanics. *J Nonlinear Sci.* 20:781–830, 2010.